

High Speed Buffered Injection Readout for Airborne Visible and Infrared Imaging Spectrometer (AVIRIS)

Bedabrata Pain, Timothy Shaw, Michael Eastwood, and Robert O. Green

Jet Propulsion Laboratory, California Institute of Technology
4800 Oak Grove Drive, MS 300-315, Pasadena, CA 91109-8099
Tel: (818)-354-8765, Email: bpain@jpl.nasa.gov

ABSTRACT

Design and operation of a high speed, low noise, wide dynamic range linear infrared multiplexer array for readout of infrared detectors with large detector capacitance is presented. Image lag related to abrupt transitions of signal currents is analyzed. A software error correction algorithm, along with its shortcomings is described. Pixel amplifier design considerations for high speed operation with reduced image lag is presented. Measured performance indicates that pixel amplifier design improvements have led to 2-3 times increase in signal-to-noise ratio, and reduction of image lag to less than 10 % over the entire dynamic range of 10 pA to 10 nA of signal. Measured input referred noise is less than 300 electrons.

Keywords: large dynamic range, focal plane arrays, readout electronics, imaging spectrometer, high speed readout, buffered direct injection.

1. INTRODUCTION

Great advances have been made in infrared focal plane multiplexer technology in the last decade. Infrared multiplexer design is just as diverse as the nature of applications and wavelength of operation. Large format (1024x1024) multiplexers with small pixel pitch ($< 20 \mu\text{m}$) and low noise ($< 30 e^-$) have been demonstrated for SWIR and MWIR imaging applications. Medium format (e.g. 640x480) multiplexers are available for LWIR tactical and earth observing applications where large signal handling capacity is an important requirement. Most staring focal planes found in imaging applications usually operate with sufficient integration times in order to improve signal-to-noise ratio. On the other hand, for airborne applications, choice of exposure time represents a trade between tolerable motion blur and required signal-to-noise ratio. Time-delay-integration is one method to achieve very low noise by increasing the effective integration time without introducing motion blur. Very low noise, high speed TDI multiplexer have been reported previously. For airborne spectrometry applications, focal plane design has to additionally contend with more stringent requirement on signal-to-noise ratio, since in contrast with an imager system, amount of signal collected by each detector for spectrometric applications diminishes at least by the number of spectral channels. The problem is even more acute for an imaging spectrometer, since the use of a mechanical scanning arrangement precludes the use of TDI technique for enhancing signal-to-noise ratio. Thus, for increasing signal-to-noise ratio, detector size is increased, consequently increasing the detector capacitance. Achieving low noise readout at short exposure times and with a large detector capacitance creates major challenges for focal plane multiplexer design.

In this paper, we present the design and performance of a high speed, low noise, wide dynamic range linear infrared multiplexer array for readout of infrared detectors with large detector capacitance. The focal plane is integrated in an imaging spectrometer called AVIRIS. The paper is organized as follows. In the next section, a brief description of AVIRIS instrument and the focal plane requirements are presented. Section 3 presents a description of the readout circuit, along with the image lag problem associated with operation at short exposure time and large detector capacitance. Section 4 presents a software correction algorithm and its shortcomings. Section 5 details the amplifier design, followed by section 6 that discusses the results and identifies unresolved problems.

2. AIRBORNE VISIBLE/INFRARED IMAGING SPECTROMETER

Spectroscopy has been used in the laboratory and on the ground for science research as well as applications for more than 100 years. NASA's Airborne Visible/Infrared Imaging Spectrometer (AVIRIS) was conceived for the same purpose, but from an Earth remote sensing perspective [1]. AVIRIS measures the solar reflected spectrum from 400 to 2500 nm at 10 nm intervals. These spectra are measured as images with 20 m spatial resolution and an regional coverage of 11 by up to 800 km. The AVIRIS sensor flies on a NASA ER-2 aircraft at an altitude of 20 km. The quality of the spectral images allows AVIRIS to contribute to science research and applications spanning the disciplines of: atmospheric correction, ecology and vegetation, geology and soils, inland and coastal waters, the atmosphere, snow and ice hydrology, biomass burning, environmental hazards, satellite simulation and calibration, commercial applications, spectral algorithms, urban and human infrastructure, as well as spectral modeling. Continuous advances in the AVIRIS sensor and data system leave AVIRIS with an unparalleled spectral, radiometric, spatial calibration in conjunction with high signal-to noise.

The instrument consists of four focal planes each consisting of a linear array of detectors hybridized to readout multiplexers. Each focal plane consists of 64 detectors, providing a total of 224 spectral band information for each ground pixel. The scanning mirror arrangement covers 614 ground pixels cross-track per scan. In order to prevent motion blur, the exposure per ground pixel is limited to less than 87.5 μ sec. Both silicon and InSb photodiode arrays are used to cover the visible/SWIR waveband, silicon being used for visible end of the spectrum. In order to achieve sufficient signal to noise ratio, the detector sizes vary from 200 μ m x 200 μ m to 200 μ m x 400 μ m, causing the detector capacitance to be in the range of 10pF to 30 pF. The focal plane operates at liquid nitrogen temperature of 77 K. Depending upon the phenomena being observed, the detector current and the signal handling capacity can vary by many orders of magnitude. Instantaneous detector current range in a given detector can vary from 2 pA to 5 nA, i.e. by 68 dB. The required read noise is around 500 e^- , corresponding to $\frac{1}{2}$ the minimum detectable signal. Both types of detectors were built by Cincinnati Electronics which also carried out the entire focal plane assembly as well as the initial focal plane readout circuit design [2].

3. UNIT CELL DESCRIPTION AND IMAGE LAG

The focal plane readout consists of a linear array of 1x64 multiplexers, with the unit cell consisting of a buffered direct injection (BDI) input [3], and a readout signal chain – shown schematically in Figure 1. Schematically, the detector is represented by a current source in parallel with a resistor and a capacitor. Both InSb and silicon detectors have large detector resistance (> 10 G Ω). The signal chain consists of a chain of source followers (shown schematically in figure 1 as triangles)

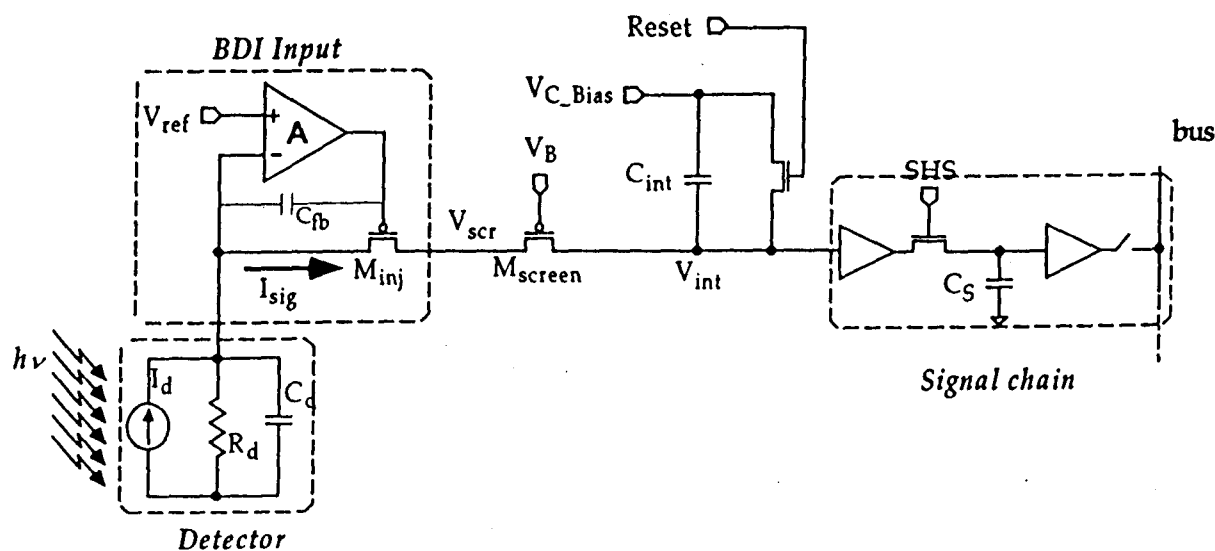


Figure 1. AVIRIS readout unit cell circuit with signal chain.

representing generic amplifiers) along with sampling capacitors (C_s). Every 87.45 μsec . (i.e the exposure time), all 64 unit cell outputs are simultaneously sampled into their respective sampling capacitors to ensure snap-shot mode of operation. The multiplexed source followers that are clocked to provide data output at 750 kHz rate. The focal plane readout described in this paper uses the same digital control logic as in the initial Cincinnati Electronics design, but the unit cell electronics has been changed [4].

The BDI input circuit consists of a differential amplifier providing feedback to ensure minimal swing at the detector node, while injecting the photocurrent through the injection FET (M_{inj}) into the integration capacitor (C_{int}) with high injection efficiency at high speed. In order to reduce errors due to channel length modulation (i.e. finite output impedance), a screen FET (M_{screen}) is introduced between M_{inj} and C_{int} . The screen FET acts as a cascode transistor to hold the drain of M_{inj} (V_{scr}) constant. The maximum linear signal swing at V_{int} is determined by the bias on M_{screen} (V_B). For proper operation, M_{screen} is biased in saturation. Since in weak inversion, saturation is achieved for $|V_{ds}| \sim 5\phi_T$, where ϕ_T is the thermal potential, maximum linear swing at $V_{int} \sim V_B + |V_T| - 5\phi_T$. Choice of C_{int} represents a trade between maximum signal handling capacity ($\sim C_{int}$), transfer gain ($\sim 1/C_{int}$), and conversion linearity ($\sim C_{int}$). In this focal plane, C_{int} is chosen to be 0.2 pF.

Nominally, BDI input is needed for readout of detectors with small detector resistance, a situation commonly encountered in MWIR or LWIR applications. A BDI input circuit allows the input impedance (Z_{rdo}) of the readout multiplexer circuit to be much smaller than the detector impedance (Z_d) so that the photocurrent is not integrated on the detector itself, but is injected into the readout circuit. The BDI input circuit reduces the effective input capacitance by minimizing voltage variations at the detector node through feedback with a differential amplifier with high gain A . The effectiveness of the input circuit to couple the photocurrent into the readout circuit is measured by injection efficiency (η), defined as:

$$\eta = \eta_o \frac{1}{1 + j\frac{f}{f_c}} = \frac{I_{sig}}{I_d} \cdot \frac{1}{1 + j\frac{f}{f_c}} \quad (1)$$

where, I_{sig} is the injected current through M_{inj} in response to detector current I_d . Cut-off frequency (f_c) depends in a complicated way on the transconductance of M_{inj} , detector current, on detector capacitance, and on amplifier gain (A).

For AVIRIS, both detector resistance (R_d) and capacitance (C_d) is very large. A large detector resistance allows the d.c. component of the injection efficiency to be nearly unity, while a high detector capacitance reduces the cut-off frequency for the injection efficiency, causing problems for circuit operation at high speed or with short exposure times. The problem is apparent when the detector current varies by a large amount between frames, as shown in the simulation in figure 2. Figure 2 shows the response of injected current (I_{sig}) to a variation of the detector current from 1 nA in one frame to 0.1 nA in the next, each frame being 200 μsec . in duration, and the readout is operated in the direct injection mode to accentuate the phenomenon. A large detector capacitance prevents the detector node from being charged or discharged at high speed, causing I_{sig} to always lag behind I_d . Retention of charges on the detector caused by a large response time constant produces an output that depends on the amount of detector current from the previous frame, causing the appearance of "ghost" image.

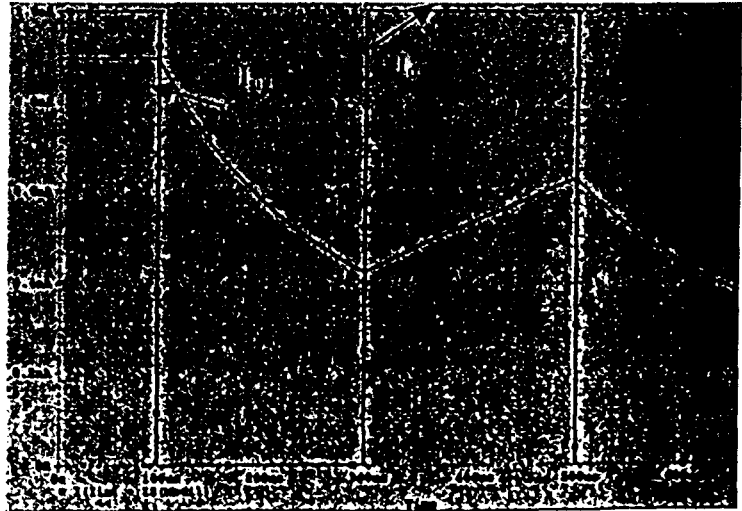


Figure 2. Simulated injected current for pulsed detector current

The effect of image lag or residual image on spectrometer performance is demonstrated in figure 3. It shows the AVIRIS

focal plane output for different channels, each channel representing a different ground pixel during the cross-track mechanical scan. For each channel, figure 3 plots the response from 3 proximate detectors, representing 3 spectral bands. The response of one of the detectors (# 174) corresponds to CO₂ absorption band, and is hence much lower in intensity than the other two, that lie outside the absorption band. The dip in the response in the middle corresponds to the ground pixel intensity variation. The plot shows that for the same relative variation in ground pixel intensity, percentage change in focal plane output varies from one detector to another, the variation being dependent on the steady-state output level in the detectors. The dependence of the output in a given frame on the steady-state output level is an evidence of the image lag. The presence of residual image causes significant errors in estimation of ground and atmospheric constituents, which involve computation of ratios of detector outputs.

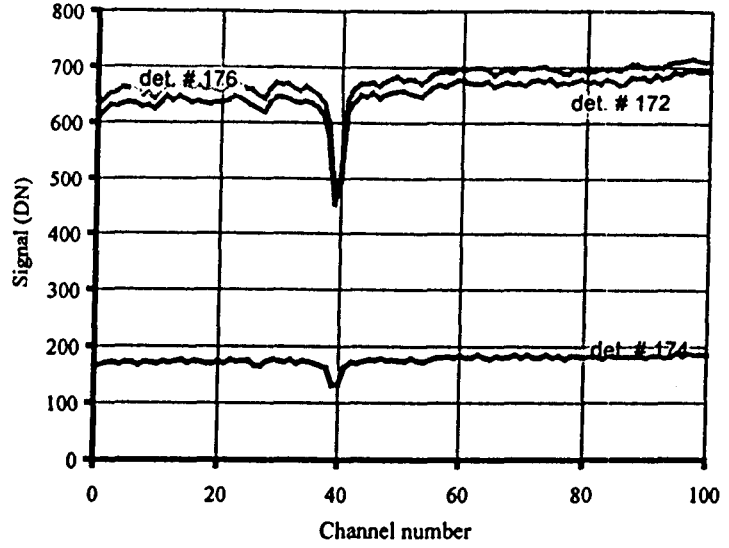


Figure 3. Outputs from three adjacent detectors as a function of channel numbers

4. SOFTWARE CORRECTION

The error in measurement is due to the inability of the input circuit to drain out charges from the detector fast enough compared to the exposure time (t_{int}). However, since charge in the detector-readout system is conserved, it is possible, at least in principle, to recursively estimate and correct the measurement errors. For software correction, it is assumed that the current injection from the detector can be modeled by a first order system response. Specifically,

$$I_{sig} = I_d + C_d \cdot \frac{dv_d}{dt} \quad (2)$$

where v_d is the instantaneous detector potential. The differential equation can be solved to yield (after addition of appropriate boundary conditions):

$$Q_{sig}(k) = [1 - \alpha(k)] \cdot Q_d(k) + \alpha(k) \cdot Q_{err}(k) \quad (3)$$

where $Q_{sig}(k)$ is the total charge integrated on C_{int} during k -th exposure, $Q_d(k)$ is the total charge added to the detection system during the k -th exposure interval by a fixed detector current flowing during the interval, $Q_{err}(k) = I_{sig}(k) \cdot t_{int}$, with $I_{sig}(k)$

is the current through M_{inj} at the beginning of the k -th exposure interval, $\alpha(k) = \frac{\tau(k)}{t_{int}} \left[1 - \exp\left(-\frac{t_{int}}{\tau(k)}\right) \right]$,

and $\tau(k) = \frac{A \cdot g_{minj}}{C_d + A \cdot C_{gs}}$, with C_{gs} being the injection FET gate-to-source capacitance, and g_{minj} is its transconductance.

In order to complete the recursion, $Q_e(k)$ must be expanded to explicitly include its dependence on the detector current during the $(k-1)$ th exposure cycle. Equating the current flow through the injection FET during the two exposure frames, $Q_{err}(k)$ can be written as:

$$Q_{err}(k) = [1 - \beta(k-1)] \cdot Q_d(k-1) + \beta(k-1) \cdot Q_{err}(k-1) \quad (4)$$

where $\beta(k) = \exp[-t_{int}/\tau(k)]$. Using the recursive relations described though the coupled equations 3 and 4, the actual amount of charge added to the system ($Q_d(k)$) can be estimated, providing the error correction.

The error correction was implemented in software and was applied to a large amount of data collected by AVIRIS. Figure 4 shows the effect of error correction on the data shown in figure 3. To estimate the accuracy of error correction, ratio of signal in detector # 174 to the sum of the signals in detectors # 172 and # 176 are computed on the data before and after correction. This ratio represents the relative abundance of CO₂ in the atmosphere over the terrain where the AVIRIS collected the data. Since CO₂ concentration is relatively fixed, the ratio should be independent of the ground pixel intensity. As shown in figure 4, the spikes in the relative concentration computed from the raw (uncorrected) data represent errors due to image retention. Although the spikes are reduced in the software corrected data (open dots), a number of false spikes have also appeared, indicating inadequacy of the algorithm. The inability to correct errors is due both to modeling shortcomings as well as inaccuracies in the estimation of circuit time constants. Proper modeling requires a complicated second order system description, making the correction algorithm difficult to implement.

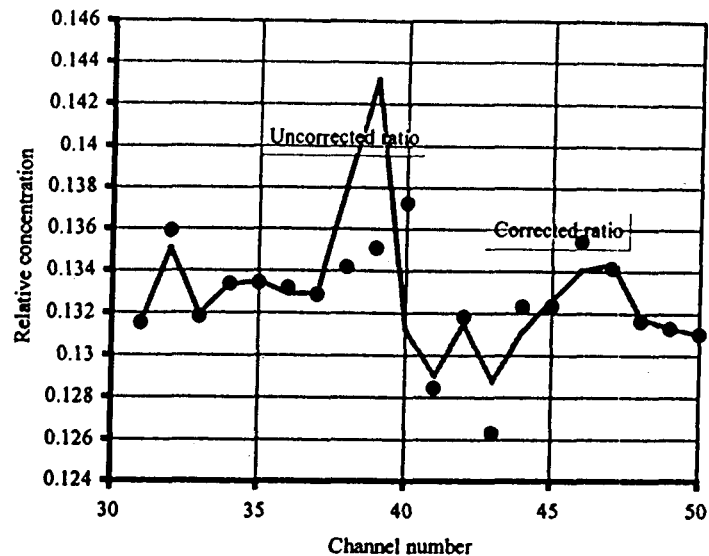


Figure 4. Relative abundance of CO₂ as a function of channel number calculated from raw and corrected data set

5. AMPLIFIER DESIGN & OPERATION

5.1 Differential amplifier design

A BDI input circuit requires a high gain amplifier to provide appropriate feedback. A differential amplifier implementation is chosen in order to have accurate detector bias control, the detector node being set to V_{ref} for high gain feedback. In order to achieve high injection efficiency at high speeds, the amplifier needs both high gain and high cut-off frequency. Figure 5 shows the schematic of the differential amplifier initially used for the focal plane. The single-ended amplifier consists of a pair of n-channel input MOSFETs, a pair of n-channel cascode MOSFETs, and current-mirror p-channel load. In order to achieve high-speed BDI operation, the amplifier output resistance is kept low to maximize amplifier cut-off frequency (f_c).

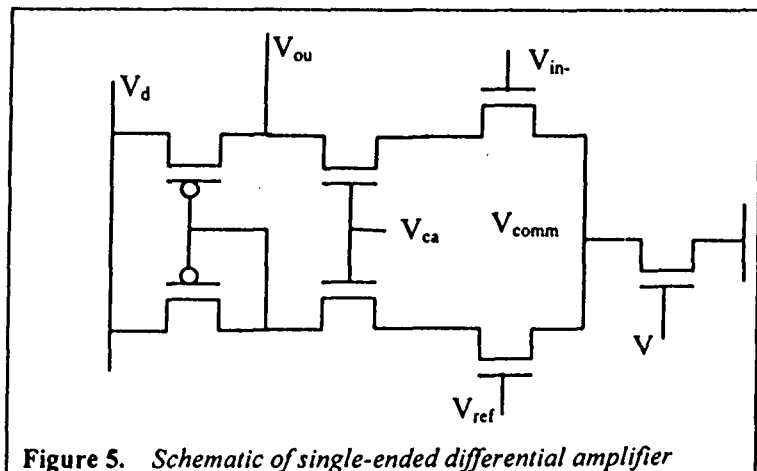


Figure 5. Schematic of single-ended differential amplifier

The gain of the simple single-ended amplifier is around 700 (56 dB) at 77K. The gain is kept high by increasing the input transistor size, thereby increasing its transconductance (g_m), and by using FETs with long device lengths to minimize short channel effects, thereby providing large output resistance. At lower temperatures, FET g_m increases primarily due to increase in mobility, providing higher gain over room-temperature operation. Since large sized transistors are used to implement the amplifier, a cascode input configuration is chosen for minimization of input-to-output capacitance, required for high speed settling.

The effective input capacitance because of the amplifier feedback is given by:

$$C_{eff} \approx \frac{C_d}{A} \quad (5)$$

Equation 5 indicates that a gain of 700 is enough to allow the effective input capacitance to be ~ 50 fF, that is smaller than the integration capacitance. Hence, a gain of 700 is sufficient for BDI operation. However, one of the problems of this circuit

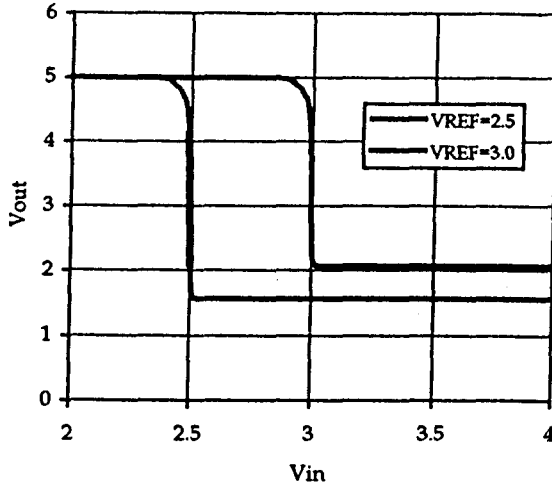


Figure 6. DC transfer characteristics of the differential amplifier

is that it does not provide proper feedback due to improper level shifting inherent to the operation of the opamp. Figure 6 shows the d.c. transfer characteristics of the amplifier for two values of V_{ref} as V_{in} is swept from 0 to 5V. It indicates the amplifier does not provide output with rail-to-rail voltage swing. When $V_{in} > V_{ref}$, the minimum output depends on V_{ref} , and is given by:

$$V_{out,min} \sim V_{ref} - V_T \quad (6)$$

where V_T is the threshold voltage of the input FET. The minimum output is pegged since a lower output voltage will not be able to keep the current in the inactive branch low. For BDI operation with a p-FET injection transistor, shown in figure 1, the output of the amplifier must be lower than the voltage on its inverting input in order to allow current injection. Figure 6 indicates that such a condition is met only when the differential amplifier operates in a low-gain region – near or at the flat part of the curve. Lack of rail-to-rail operation and output level shifting in the wrong direction causes the amplifier to bias-up the readout circuit in a pseudo

direct injection (DI) mode, negating the advantages of BDI. As a result, the detector node fluctuates by several mV, giving rise to the image lag described in section 3.

Fortunately, the problem is not fundamental, and can be easily corrected by designing the amplifier with a pair of p-input FET. The circuit topology remains, except that all the transistor flavors are inverted (p-FETs become n-FETs, and vice-versa). Consequently, the transfer curve also shifts. Rail-to-rail output swing is still not achieved, but unlike the n-input amplifier situation, the output can swing down to ground for $V_{in} > V_{ref}$, whereas for $V_{in} < V_{ref}$, the output does not swing all the way to V_{dd} . Thus, the level-shift is in the correct direction, forcing the amplifier to be biased in the high gain region when used in the BDI circuit shown in figure 1. The amplifier input transistor sizes are increased to provide the same gain as before, since p-channel FET mobility is less than that of an n-channel FET.

5.2 Effect of feedback capacitance

The transient behavior of the BDI input circuit depends on the detector current levels. The transient response is much faster for a detector current transition from low-to-high than for the opposite type transition. This is because the effective time constant varies by many orders of magnitude, since instantaneous transconductance of the injection FET is proportional to the current flowing through it. When the detector drops suddenly, the FET transconductance reduces as well, and the time constant is long. On the other hand when the detector current rises suddenly, the injection FET

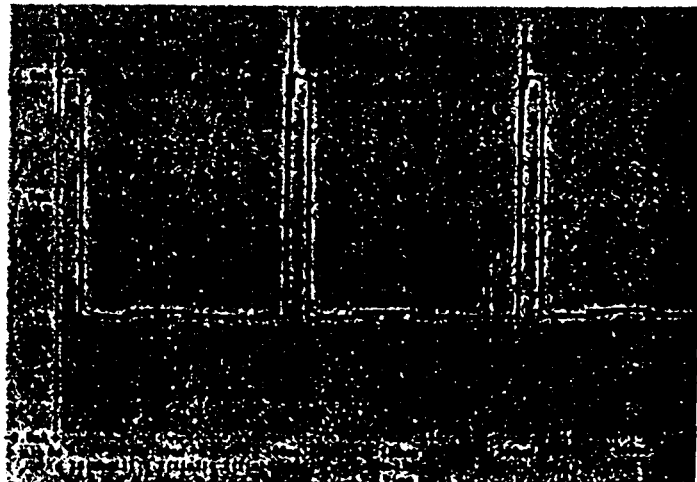


Figure 7. Effect of feedback capacitance on transient response

transconductance rises sharply so that it is comparable to the amplifier time constant. Proximity of these two poles make the BDI input circuit response oscillatory as shown in the simulations depicted in figure 7. In order to minimize the overshoots during the rising transitions, a small feedback capacitance (C_b) of 50 fF is introduced, as shown in figure 1. Simulations indicate that the feedback capacitance is small enough to reduce the oscillatory behavior without affecting the time constant for the down-going transition.

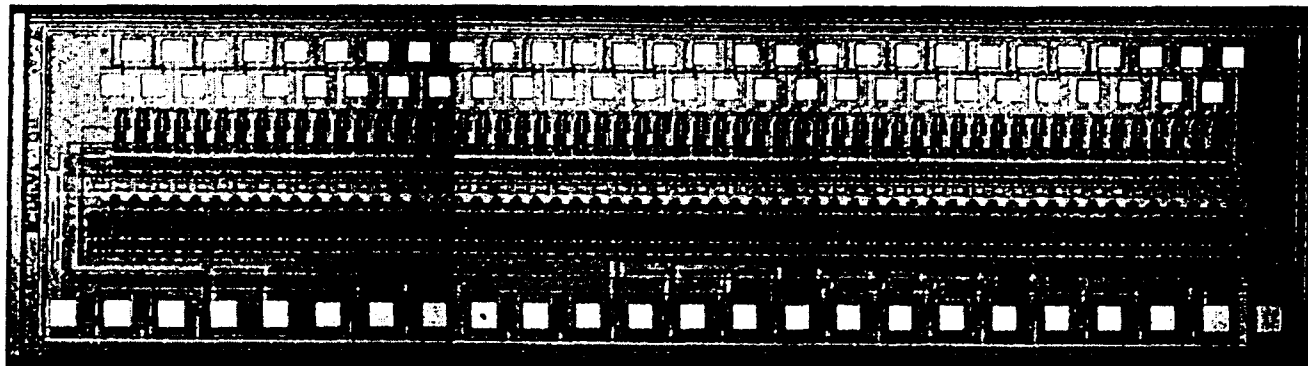


Figure 8. AVIRIS focal plane readout chip photograph

6. RESULTS

The focal-plane multiplexer was designed in 1.2 μm CMOS process from the Hewlett-Packard foundry, made available through MOSIS. The choice of 1.2 μm CMOS technology was dictated by the need for 5 V focal plane operation. Figure 8 shows the photograph of the focal plane chip. The size of the 7.1 mm x 2.2 mm, and it consists of a 64x1 readout multiplexer, 64x1 array of sampling capacitors and multiplexed analog signal chain, bias generation circuits, and digital control that provides bi-directional scan of the multiplexer, and allows operation with a minimal set of commands. The unit-cell size is 80 μm x 240 μm , including the analog signal chain, and can be reduced if necessary. For AVIRIS operation, the size of the detectors is much larger than that of unit cell readout circuit, the largest detectors being 400 μm x 300 μm in size. A fan-out boards allows connection of the larger sized detector array to the smaller sized focal plane readout array. The color shading in the picture is an artifact of the microscope camera through which the picture is taken.

6.1 Cryogenic FET operation

Unlike at room-temperatures, the amplifier gain falls linearly with bias current at low temperatures. The measured gain at 77 K was ~ 600 over current bias range of 50 - 200 μA . At or near room temperatures, amplifier gain falls off quadratically with bias current, since transconductance varies as the square-root of the bias current, and the output conductance varies linearly. However, at 77 K the transconductance is nearly independent of bias current, since an increase in mobility at lower temperatures allow velocity saturation to be reached at lower electric fields. For a device operating under velocity saturation, maximum transconductance is reached, since the vertical field can no longer affect the average velocity of the carriers in the

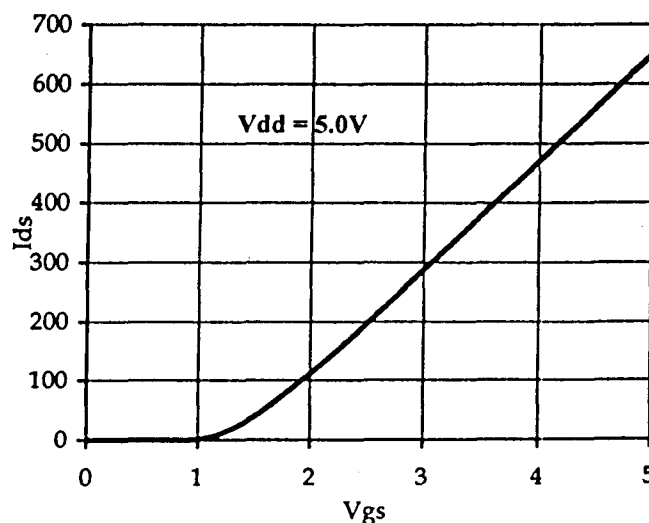


Figure 9. Drain current transfer characteristics of n-FET operated at 77 K

channel. Figure 9 shows the measured I_{ds} - V_{gs} data for a n-MOSFET (with $W/L = 1.8 \mu\text{m}/1.2\mu\text{m}$) operating at 77K. Above the threshold, the curve is linear indicating that device operates under velocity saturation. Only at very low biases do the curves show non-linearity, indicating conventional FET operation.

6.2 Signal to noise ratio

AVIRIS signal-to-noise ratio has increased continuously over the years, both due to better instrument calibration and due to improvements in focal plane design as shown in figure 10. Figure 10 shows that between 1987 when AVIRIS was first flown and 1997, the signal to noise ratio has improved by 20 times at every spectral band. The increase in signal to noise ratio was increased between 2-3 times by changing the pixel amplifier design as described in section 5, the amplifier design change enabling the

circuit to operate in BDI mode rather than in DI mode. The measured noise floor from the circuit operating in BDI mode is ~300 electrons, indicating that the noise is limited by the analog signal chain and not by the pixel read noise. The signal chain circuit is currently designed to operated in single-ended mode, causing extraneous noise pick up. Additionally, no correlated

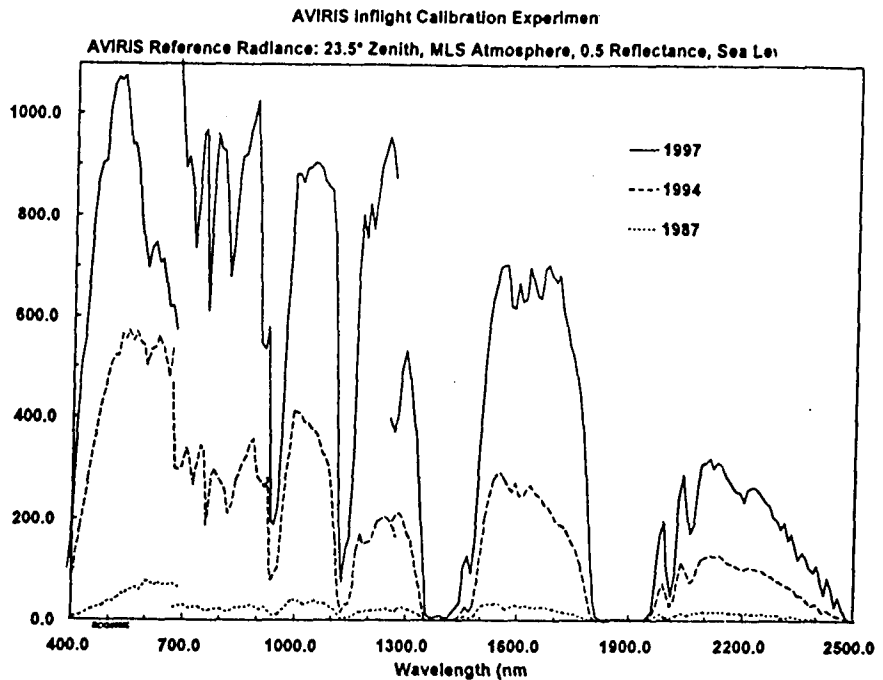


Figure 11. AVIRIS noise data at different wavelengths (measured in-flight)

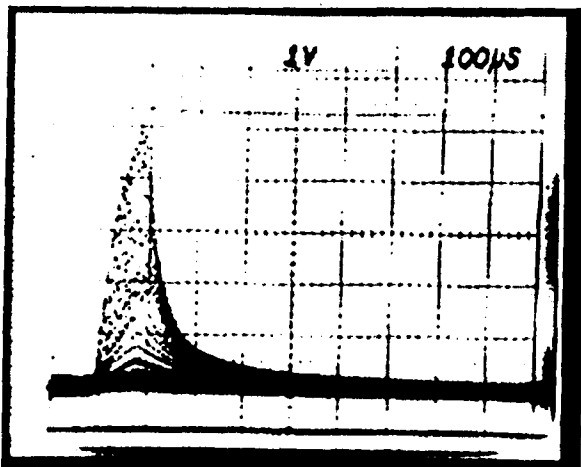


Figure 12a. pseudo-DI mode of operation

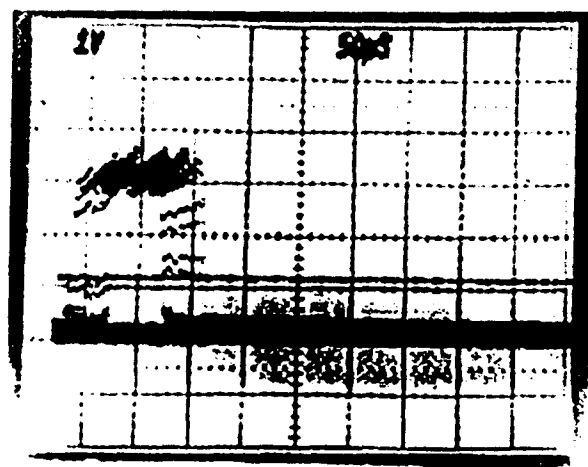


Figure 12b. BDI mode of operation

Figure 12. Scope photograph showing the response of the focal plane to asynchronously strobed radiation pulse

double sampling (CDS) is performed at the pixel level. In absence of CDS, the reset noise from the integration capacitor is about 100 electrons. Noise reduction can be achieved by a differential readout scheme that also incorporates CDS. The focal plane characteristics are summarized in table 1.

6.2 Residual image

Residual image is experimentally measured by illuminating the focal plane with an asynchronous strobe of IR radiation, the

strobe duration being much shorter than one exposure (87.45 $\mu\text{sec.}$). The asynchronous strobe allows the radiation pulse to be randomly positioned within the exposure interval. Multiple repetitions of the strobe operation causes the focal plane to generate an output whose envelope corresponds to the response time of the unit cell in response to abrupt signal change from high to low and vice versa. Figure 12 shows the response envelope for both focal planes, one which operates in pseudo-DI mode (figure 12a), and the other which operates in BDI mode (figure 12b). Between figure 12a and 12b, the time resolution is changed from 100 $\mu\text{sec.}$ to 50 $\mu\text{sec.}$ in order to better resolve faster responses with BDI unit cell. A band-limiting filter is applied on the focal plane (shown in figure 12a) to display output from one pixel. This is done to minimize envelope clutter, especially when the response times are longer than the exposure time.

For the focal plane designed with pixel amplifier that forces the input circuit to operate in pseudo-DI mode, the response is slow enough that the focal plane output never reaches steady state. The response time constant associated with pseudo-DI mode of operation is 150 $\mu\text{sec.}$ for down-going transition of detector current. Furthermore, an extend tail stretching more than 600 $\mu\text{sec.}$ is observed. This is to be expected since the instantaneous transconductance of the injection FET reduces linearly with the current through it, causing the response curve to be stretched. For the second focal plane where BDI mode of operation is established, the response time constant reduces to less than 15 $\mu\text{sec.}$ due to feedback that reduces the effective capacitance. No anomalous decay behavior (stretched response curve) is present, although there is an unexplained undershoot.

In spite of reduction of image lag as shown in figure 12b, further improvement in residual image is desirable and possible. That will require redesign of the pixel amplifier to provide higher gain, greater phase margin and higher cut-off frequency. An amplifier design that meets these characteristics can be implemented for linear arrays, although will be difficult for 2-D array imaging type applications.

7. CONCLUSIONS

Design and operation of a high speed, low noise, wide dynamic range linear infrared multiplexer array for readout of infrared detectors with large detector capacitance. An analysis of image lag effects due to short exposure with high capacitance detectors is presented. A software error correction algorithm and its shortcomings are presented. Pixel amplifier design considerations for high speed operation with reduced image lag is described. Measured performance indicates that pixel amplifier design improvements have led to 2-3 times increase in signal-to-noise ratio, and reduction of image lag to less than 10 % over the entire dynamic range of 10 pA to 10 nA of signal. Measured input referred noise is less than 300 electrons.

8. ACKNOWLEDGEMENTS

This research was carried out at the Jet Propulsion Laboratory/California Institute of Technology, Pasadena, California, under contract with the National Aeronautics and Space Administration. The authors would like to thank Cincinnati Electronics for providing detectors, for carrying out packaging, for designing the digital control logic. The authors also extend their thanks to Dr. Guang Yang, Dr. Thomas Cunningham, Mr. Mike Fitzsimmons, Mr. John Koehler, and Mr. Monico Ortiz at JPL for insightful discussions and their helps in various aspects of design, design-reviews, and testing.

9. REFERENCES

1. Airborne visible/Infrared imaging spectrometer, A description of the sensor, ground data, processing facility, laboratory calibration, and first results, Gregg Vane, ed., JPL publication, 87-38, 1987.
2. C.A. Niblack, M.A. Blessinger, A.P. Westrick, M.L. Eastwood, and C.O. Staller, "Multiplexed focal plane array upgrade for the AVIRIS instrument", in *Infrared detectors and Instrumentation*, Proc. SPIE, vol. 1946, pp. 341-348, 1993.

3. M. A. Blessinger, "Comparative study of linear multiplexer for a remote sensing applications", in *Infrared Readout Electronics II*, Proc. SPIE, , vol. 2226, pp. 172-179, 1994.
4. B. Pain, S.K. Mendis, R.H. Nixon, and E.R. Fossum, "Low light level active pixel sensor with on-chip signal processing", in *Surveillance Technologies and Imaging Components*, Proc. SPIE vol. 1952, pp. 23-33, 1993.
5. N. Bluzer and A. Jensen, "Current readout of infrared detectors", *Optical Engineering*, vol. 26, no. 3, pp. 241-248, 1987.
6. M. Nelson, J. F. Johnson and T. S. Lomheim, "General noise processes in hybrid infrared focal plane arrays", *Optical Engineering*, vol. 30, no. 11, pp 1682-1699, 1991.